Available online at www.sciencedirect.com
ScienceDirect
Trans. Nonferrous Met. Soc. China 34(2024) 1214−1225
Transactions of Nonferrous Metals Society of China
www.tnmsc.cn

Cryogenic rolling impacts on microstructures and properties of a novel Ni−W−Co−Ta medium-heavy alloy

Kang-hao SHU[1], Yi XIONG[1,2], Yong LI[3], Yun YUE[1], Zheng-ge CHEN[4], Xiao-qin ZHA[5], Shun HAN[3], Chun-xu WANG[3]

1. School of Materials Science and Engineering, Henan University of Science and Technology, Luoyang 471023, China;
2. Collaborative Innovation Center of New Nonferrous Metal Materials and Advanced Processing Technology, Luoyang 471023, China;
3. Research Institute of Special Steels, Central Iron and Steel Research Institute Company Limited, Beijing 100081, China;
4. State Key Laboratory of Laser Interaction with Matter, Northwest Institute of Nuclear Technology, Xi'an 710024, China;
5. Luoyang Ship Material Research Institute, Luoyang 471000, China

Received 08 October 2022; accepted 12 April 2023

Abstract: A high-strength Ni−W−Co−Ta medium-heavy alloy (MHA) was prepared through the melting–casting–forging followed by cryogenic rolling process. Detailed microstructure and mechanical property characterizations were conducted to unveil the influence of cyrorolling on Ni−W−Co−Ta MHA. The results revealed that initial equiaxial grains were elongated along the rolling direction firstly and then transformed to fibrous texture with increase in accumulated deformation, in which a large number of slip bands were generated to coordinate the intensive plastic deformation. A sharp increase in dislocation density significantly promoted the dislocation interactions, which, in turn, refined the grains down to nanometer scale. The strength and hardness increased significantly with the increase of the deformation, whereas the elongation decreased sharply. The fracture morphology changed from a typical ductile mode for the undeformed sample gradually to quasi-cleavage and ductile mixed mode for 90% deformed material.

Key words: Ni−W−Co−Ta medium-heavy alloys (MHAs); cryogenic rolling; fibrous texture; mechanical property; quasi-cleavage and ductile mixed fracture

1 Introduction

Warhead material usually has to suffer from high strain rate deformation (10^3−10^9 s^{-1}) coupled with high temperature and pressure because of its special service environment. It is prone to loss of striking ability resulting from the rapid failure, considering the adiabatic shearing phenomenon during high strain rate deformation [1]. Therefore, warhead material is required to have superior property features such as excellent plasticity and toughness, high strength, and high penetration [2].

At present, one of the two most commonly used warhead materials is ultrahigh-strength steel that has high toughness and strength [3−5]. However, this kind of steel is not suitable for applications such as armor-piercing shells and drilling ammunition, as its low density makes it difficult to achieve high penetration force and excellent dynamic mechanical properties [6]. The other option is tungsten (W) heavy alloys (WHAs), which have high density and penetration force [7,8]. WHAs typically contain 85−99 wt.% W as the matrix with a small amount of Ni, Cu, Fe, Co, Mo, Cr, etc. However, drawbacks of conventional WHAs,

Corresponding author: Yi XIONG, Tel: +86-379-64231269, E-mail: xiongy@haust.edu.cn
DOI: 10.1016/S1003-6326(24)66465-4

for example their low dynamic rheological stress and strength, and poor toughness, limit their application in high-end military fields [9,10]. Therefore, researchers have carried out extensive research focusing on manipulating the W contents [11] and sintering methods [12,13] of WHAs. Consequently, the mechanical properties of WHAs have been improved to some extent. Nevertheless, W is expensive and the total W reserves of the world are only 3.7 million tons [14], which limits its production and application on a large scale.

A medium heavy alloy (MHA) with medium W content (50%−75%) was proposed by YE et al [15] to reduce the costs of WHAs. It was found that the mechanical properties of MHA and WHA are comparable, and thus MHA could be a promising alternative to WHA. The aforementioned MHAs and/or WHAs were mainly manufactured by powder metallurgy method. Materials obtained by these methods always have porosities, which makes it quite challenging to apply MHAs and/or WHAs in harsh service environments [16]. Therefore, the search for novel high-density alloys with excellent comprehensive mechanical properties are still ongoing.

Recently, a novel Ni−W−Co−Ta MHA (ρ= 11.41 g/cm^3) was prepared by using Ni as the matrix and W as the strengthening phase, together with a small amount of Co and Ta [17]. The yield strength and tensile strength of this MHA after aging treatment at 750 °C for 5 h were found to be as high as 1571 and 1746 MPa, respectively. However, these values are still unable to meet the service requirements under extreme conditions. Therefore, this work aimed to further improve the comprehensive mechanical properties of this Ni−W−Co−Ta MHA by cryogenic rolling. The evolution of the microstructure and mechanical properties of Ni−W−Co−Ta MHAs with different deformation degrees induced by cryogenic rolling were systematically investigated, in order to establish an experimental basis and technical support for the preparation of ultra-fine grain Ni−W−Co−Ta MHAs with excellent properties.

2 Experimental

The experimental Ni−W−Co−Ta MHAs were prepared by casting after vacuum induction melting combined with vacuum-consumable arc melting. The measured compositions of as-cast ingots are 38.53 wt.% W, 5.09 wt.% Co, 0.97 wt.% Ta, and 55.41 wt.% Ni. The ingots were homogenized at about 1230 °C for at least 48 h to remove severe dendrites, segregation, and pores. Subsequently, the homogenized ingots were forged at 1180 °C to billets with a diameter of 60 mm, and then air-cooled to room temperature. To remove forging defects, these forged billets were heat-treated at 1000 °C for 1.5 h followed by air cooling.

The cryogenic rolling was carried out on Ni−W−Co−Ta MHA plates with a dimension of 100 mm × 40 mm × 10 mm that were cut from the center of forged billets along the forging direction. A multi-pass rolling method was adopted with a thickness reduction of approximately 2% per pass to achieve an overall thickness reduction of 30%, 50%, 70% and 90%, representing equivalent true strains of 0.4, 0.7, 1.2 and 2.3, respectively. Before each rolling pass, the rolls and specimens were immersed in liquid nitrogen. During rolling, the specimens were quickly taken out for a single pass of cryogenic rolling and then immersed again in liquid nitrogen for next pass. The prepared specimens after rolling were stored at room temperature.

Metallographic samples were prepared by following the standard metallographic methods and corresponding microstructural features were observed on the longitudinal plane, i.e. the rolling direction (RD) and normal direction (ND) plane, of rolled sheets with an OLYMPUS PMG3 optical microscope (OM) and JSM−7800F field emission scanning electron microscope (FESEM). The etchant contained 100 mL HCl, 100 mL CH_3CH_2OH, and 5 g $CuCl_2$. EBSD was carried out using JSM−7800F FESEM equipped with an Oxford-EBSD system. Samples for EBSD were prepared by mechanical polishing, followed by electropolishing in a solution of 475 mL $C_2H_4O_2$ and 25 mL $HClO_4$ at 25 °C.

A JEM−2010 transmission electron microscope (TEM) operating at 200 kV was used to further observe the microstructure evolution after cryogenic rolling. TEM thin foils were prepared from the rolled sheets on RD × TD (transverse direction) plane. A sheet with a thickness of 1 mm was firstly cut from the mid-thickness of rolled sheets, and then mechanically ground to 50 μm. Discs (d3 mm) were punched out and finally

thinned with a Gatan 691 ion thinning instrument. The phase constituents of Ni−W−Co−Ta MHAs were determined by X-ray diffraction (XRD) using a D8 ADVANCE XRD analyzer with Cu K_α (λ=0.15406 nm) X-ray source. XRD profiles were collected with a scanning step size of 0.02° in the 2θ range of 30°−100°. Hardness of Ni−W−Co−Ta MHAs was measured with a 500 g loading and a 10 s duration using an HV−1000 microhardness tester. The average of five random locations was taken as the hardness for each sample.

Dog-bone-shaped tensile specimens with a dimension of 20 mm (gauge length) × 5 mm (width) × 0.8 mm (thickness) were machined from rolled sheets along RD. Tensile tests were conducted by an Instron 5587 tensile testing machine at a loading rate of 0.1 mm/min. Tensile fracture was observed with a JSM−IT200 scanning electron microscope.

3 Results

3.1 Initial microstructure

The initial microstructure of Ni−W−Co−Ta MHA before cryogenic rolling, shown in Fig. 1(a), was dominated by equiaxed grains with an average size of about 43 μm, accompanied by a small number of annealing twins and undissolved particles. Energy-dispersive spectroscopy (EDS) analysis revealed that these undissolved particles were monolithic W (Fig. 1(b)). The EBSD inverse pole figure (IPF) revealed an average grain size of about 41 μm (Fig. 1(c)), which was slightly smaller than that determined by OM observation. In the EBSD IPF map, solid green and black lines indicate the low-angle grain boundaries (LAGBs, <15°) and high-angle grain boundaries (HAGBs, ≥15°), respectively. The estimated fraction of LAGBs and HAGBs was about 8.24% and 91.76%, respectively. Different colors, from blue to red, in the kernel average misorientation (KAM) diagram represent the differences in the degree of plastic deformation [18,19]. As shown in Fig. 1(d), the KAM or deformation strain of the undeformed Ni−W−Co−Ta MHA was small, being mainly blue that evenly distributed through the map.

3.2 Microstructural evolution after cryogenic rolling

3.2.1 X-ray diffraction patterns

The XRD patterns of Ni−W−Co−Ta MHA prior to cryogenic rolling (Fig. 2) indicated that the MHA had a single $Ni_{17}W_3$ phase (PDF# 65-4828). After cryogenic rolling, full width at half maximum (FWHM) of the diffraction peaks broadened. For

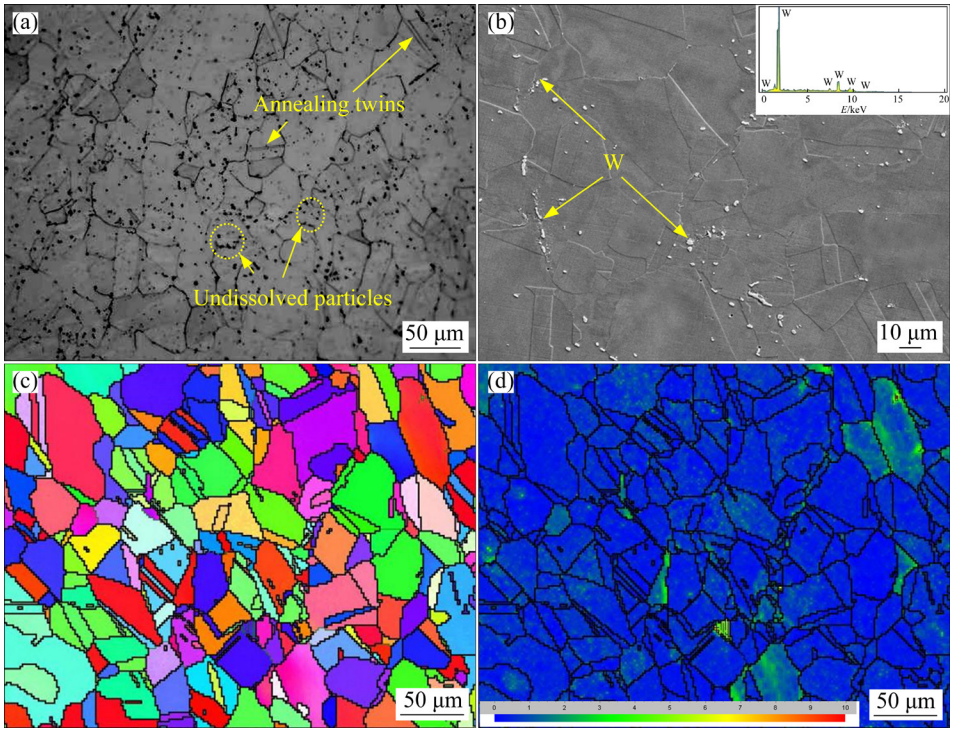

Fig. 1 Initial microstructure of Ni−W−Co−Ta MHA: (a) OM image; (b) SEM image; (c) EBSD IPF; (d) Corresponding KAM map

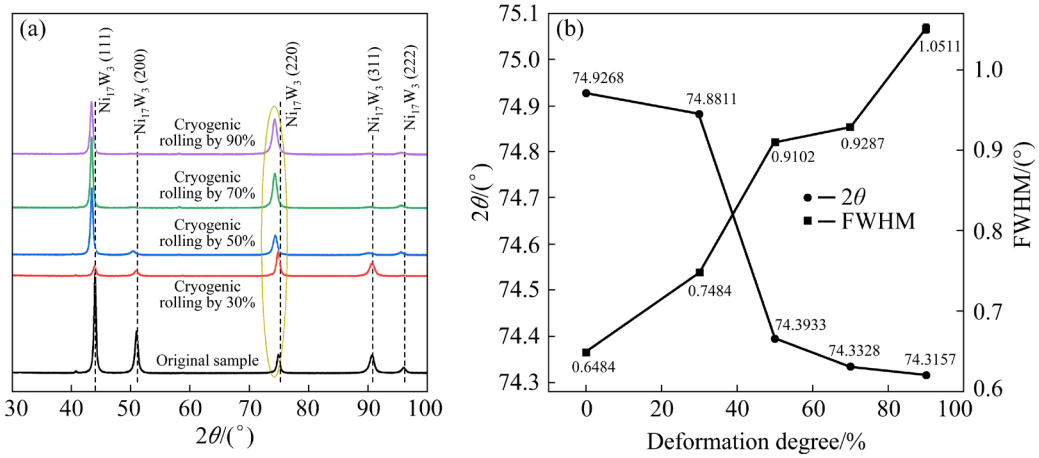

Fig. 2 XRD patterns (a) and variation in peak positions and FWHM of representative (220) plane (b) of Ni−W−Co−Ta MHAs

example, FWHM of the (220) peak increased from 0.6484° before rolling to 1.0511° after 90% reduction (Fig. 2(b)). Meanwhile, the diffraction peaks shifted to lower 2θ angles, which was associated with the accumulation of microstrain and grain refinement, similar to that found in austenitic stainless steels [20] and Al−4Mg−0.2Zr [21] after cryogenic rolling. The accumulated microstrain calculated using the W−H method [22,23] and the dislocation density [24] are shown in Fig. 3. The microstrain increased from 1.8×10^{-3} (initial) to 6.4×10^{-3} after 90% thickness reduction, whereas the lattice constant increased from 3.5785 to 3.6129 Å. The dislocation density was calculated to be 2.8×10^{14} m^{-2} at 30% reduction and increased to 2.14×10^{15} m^{-2} at 90% reduction.

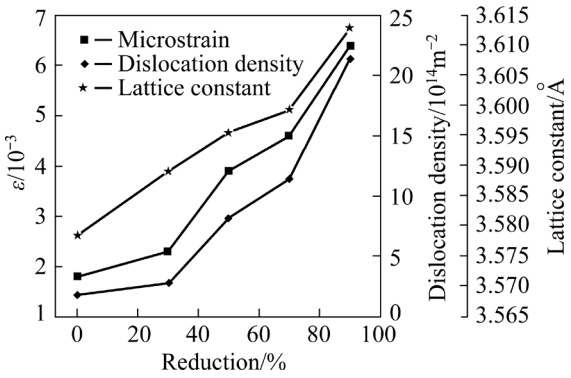

Fig. 3 Microstrain, dislocation density, and lattice constant of Ni−W−Co−Ta MHAs

3.2.2 OM and SEM results

After a thickness reduction of 30%, most of the grains were elongated along RD. A small number of undeformed grains were seen in local areas and some slip bands appeared (Figs. 4(a, b)). The number of slip bands continually increased, and the grains became further elongated and flattened along RD as the thickness reduction reached 50%. Moreover, the undissolved W particles started to be arranged to be parallel to RD (Figs. 4(c, d)). With a further reduction to 70%, the deformed grains changed from flattened shapes to strips (Fig. 4(e)). Elongated undissolved W particles were also seen along RD, as indicated in the waveform region in Fig. 4(f). Some W particles appeared to be dislodged by rolling, resulting in the formation of tiny holes (diamond marked region in Fig. 4(f)). Three different morphologies of the strips could be observed: (1) strips parallel to RD whose spacing gradually decreased with greater thickness reduction, (2) strips aligned perpendicularly to RD that were broken (elliptical region), and (3) irregularly bended strips that had a certain orientation to RD (hexagonal region in Fig. 4(f)). It was attributed to the different stress states of slip bands that, the strips of Type (1) were affected by positive stresses, those of Type (2) were gradually broken by compressive stresses, while those of Type (3) were susceptible to shear stresses and bent irregularly into a wavy shape [25].

After 90% reduction, the metallographic structure of Ni−W−Co−Ta MHA changed from strips to fibers (Fig. 4(g)). There were three different types of undissolved W particles in this case (Fig. 4(h)): (1) elongated plate-like particles along the RD (rectangular region); (2) broken particles perpendicular to the RD caused by the compressive stress during cryogenic rolling (elliptical

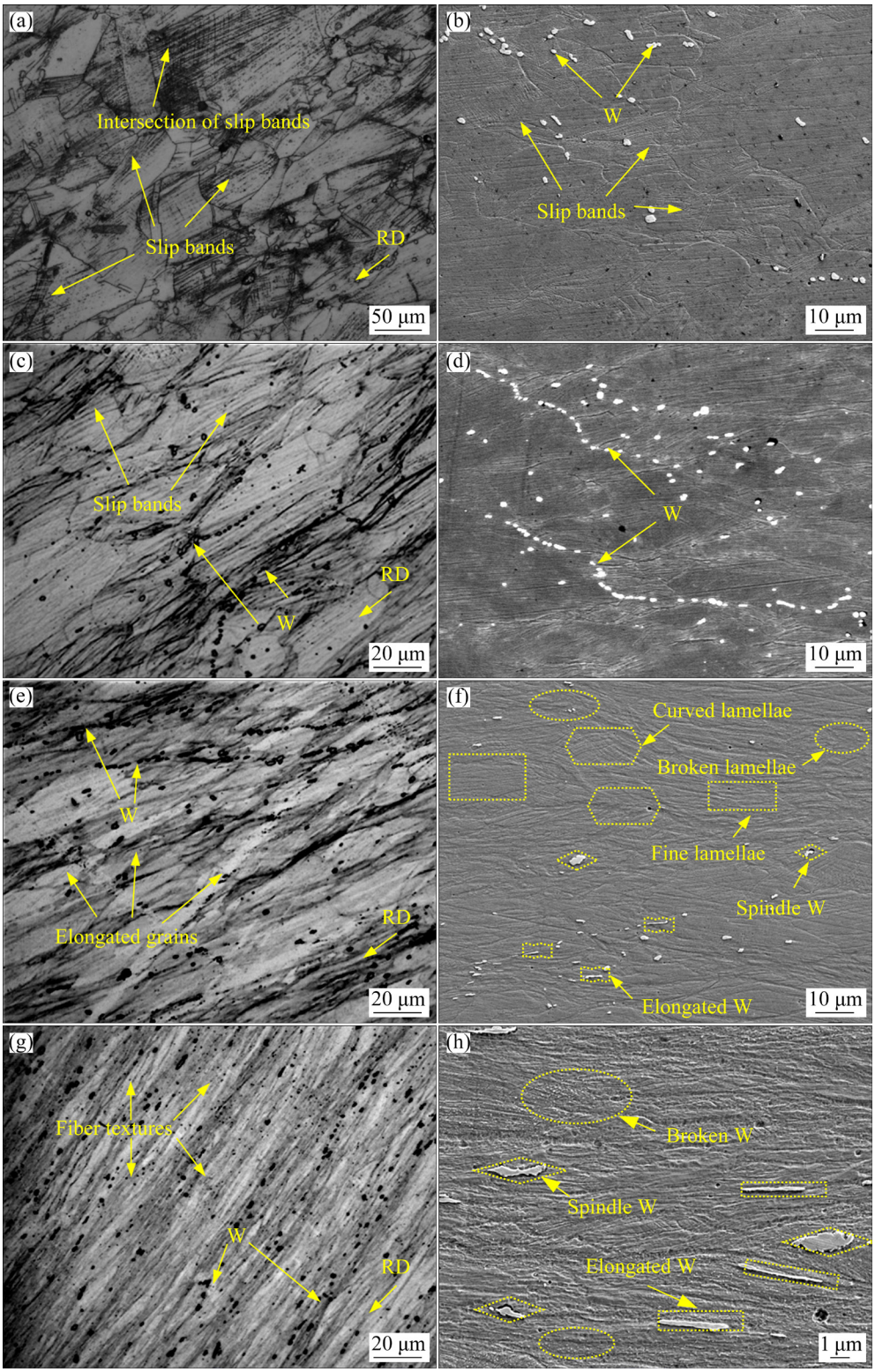

Fig. 4 OM (a, c, e, g) and SEM (b, d, f, h) characterizations of Ni−W−Co−Ta MHAs after cryogenic rolling to overall thickness reductions of 30% (a, b), 50% (c, d), 70% (e, f), and 90% (g, h)

region); (3) W particles exhibiting spindle shapes under the action of shear stress, which appeared to be dislodged to form obvious craters (diamond region). A similar microstructure composed of fine lamellae, irregularly bent and kinked slats, was also observed for pearlitic steel [26,27] and low-carbon martensite [28] as a result of heavy cold rolling.

3.2.3 EBSD results

The representative IPF of Ni−W−Co−Ta MHA after 30% reduction showed that the initial equiaxed grains were elongated along the RD, along with the presence of deformation twins and refined grains, as seen in Fig. 5(a). After 90% reduction, the grain became fragmented and refined to nanocrystals (Fig. 5(c)), similar to that in a 7050 aluminum alloy also after cryogenic rolling to a true strain of 2.3 [29]. The proportion of LAGBs increased to 83.6% at 30% reduction and 94.1% at 90% reduction, whereas that of HAGBs decreased to 16.4% (30% reduction) and 5.9% (90% reduction) (Figs. 5(a, c)). A similar phenomenon was also observed in SUS301L [30]. In addition, the average value of KAM quantitively increased to 2.1° and 2.3° (Figs. 5(b, d)) at 30%, and 90% thickness reductions, respectively. Usually, relationship between geometrically necessary dislocation density and average grain orientation difference satisfies [31]

$$\rho=\frac{\alpha\theta}{db} \tag{1}$$

where α, θ, d, and b denote a constant, average orientation value (in radian), scan step, and the magnitude of Burger's vector, respectively. It was shown that the dislocation density increases with increase in average grain orientations, qualitatively consistent with the quantified dislocation densities in Fig. 3.

3.2.4 TEM results

Figure 6(a) presents the TEM images of Ni−W−Co−Ta MHA after 30% thickness reduction. A large number of dislocations sprouted, and the dislocations interacted with each other to form dislocation tangles. Moreover, a small number of deformation twins could be observed, which could be attributed to the uncoordinated deformation between adjacent grains during cryogenic rolling [32]. A cumulative increase in strain at 50% thickness reduction resulted in an increase in dislocation density and interactions among dislocations (Fig. 6(b)), which gave rise to the formation of dislocation walls and more deformation twins, as compared with those seen at 30% deformation. Dislocation walls, tangles, and deformation twins continuously appeared in the deformed structure of Ni−W−Co−Ta MHA rolled to a thickness reduction of 70% (Figs. 6(c, d)). The bright-field (BF) images and their corresponding dark-field (DF) images at 90% thickness reduction are shown in Figs. 6(e) and 6(f), respectively. The grains were completely fragmented, and corresponding selected area electron diffraction (SAED) showed continuous rings. The grain size was estimated to be about 16.1 nm from the DF-TEM image.

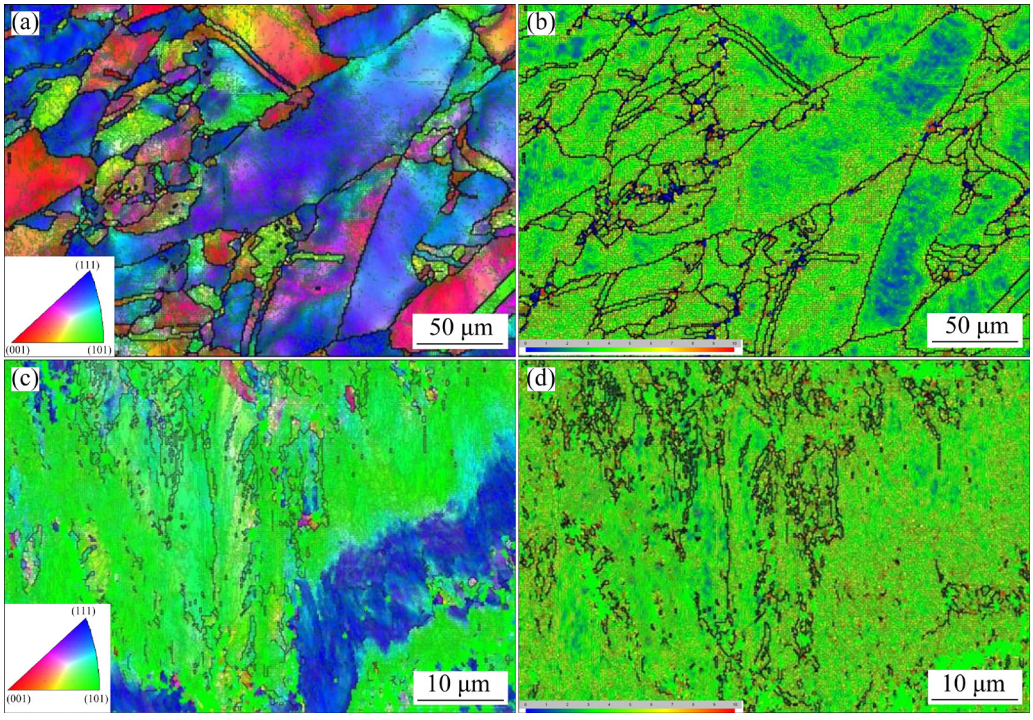

Fig. 5 EBSD IPF (a, c) and KAM maps (b, d) of Ni−W−Co−Ta MHAs after cryogenic rolling to overall thickness reductions of 30% (a, b) and 90% (c, d)

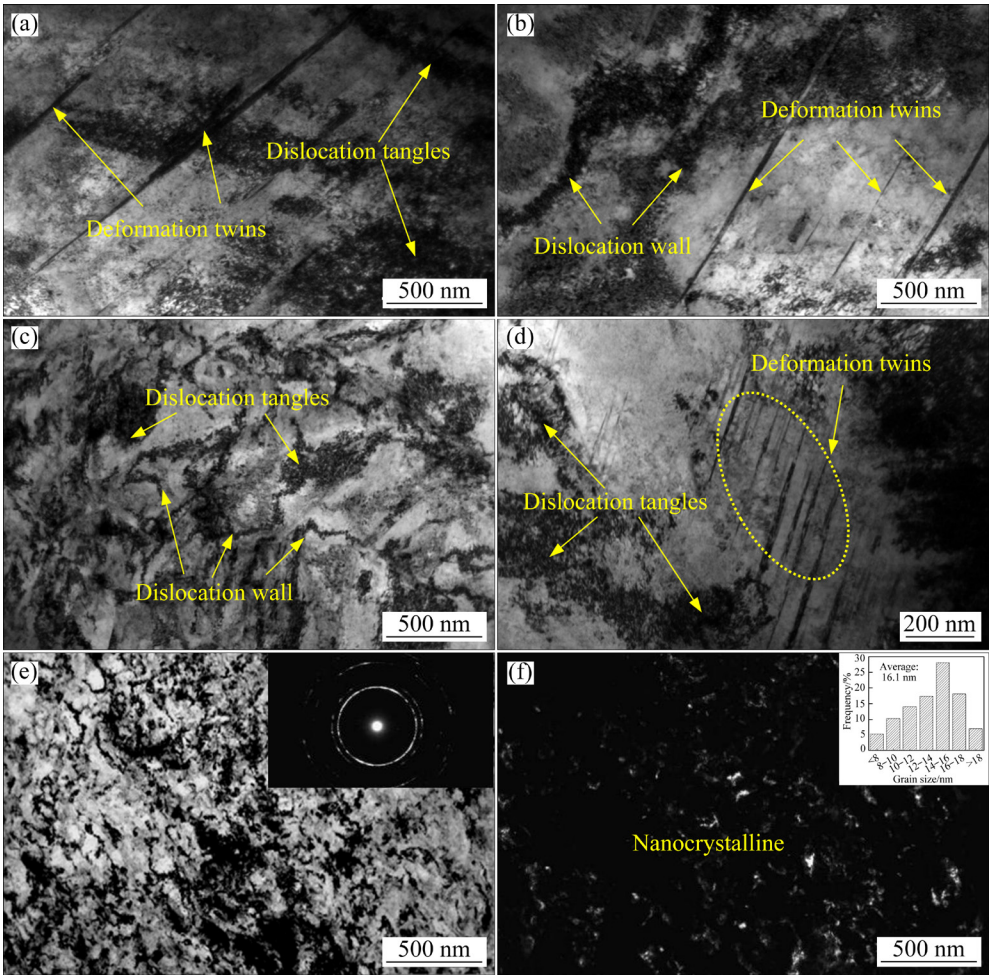

Fig. 6 TEM images of Ni−W−Co−Ta MHAs after cryogenic rolling to thickness reductions of 30% (a), 50% (b), 70% (c, d), and 90% (e, f)

3.3 Mechanical properties

Figure 7 shows the changes in microhardness and mechanical properties determined from tensile tests of Ni−W−Co−Ta MHAs. The microhardness of initial MHA was HV 292, which increased to HV 590 at 90% thickness reduction. The yield, and tensile strength values of the initial material were 505 and 978 MPa at initial condition, which increased rapidly to 2045 and 2107 MPa, by 304.9% and 115.4% after 90% thickness reduction, respectively. However, the elongation decreased sharply from 52.9% to 6.4%. This can be attributed to the rapid increase in dislocation density caused by dislocation proliferation with increase in deformation, leading to an increase in dislocation interactions and generation of dislocation jog and pileup. These are beneficial factors for the immobile dislocation. Because of grain refinement and significant increase in the grain boundaries,

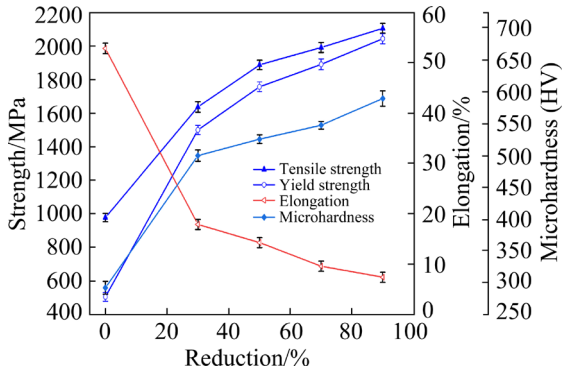

Fig. 7 Mechanical properties of Ni−W−Co−Ta MHAs after cryogenic rolling

dislocations at the grain boundaries continued to accumulate to form more dislocation tangles, resulting in an obvious stress concentration phenomenon. When the local stress concentration was large enough, new dislocations would generate in the adjacent grains to relieve the stress

concentration at grain boundaries. Therefore, with gradual grain refinement, the material contained more grain boundaries to enhance the hindrance of dislocation movement [33]. Therefore, work-hardening of the Ni−W−Co−Ta MHA occurred under the combined effect of these factors. In addition, Fig. 4 showed that the undissolved W particles became continuously elongated and gradually dislodged to form tiny holes, leading to a decrease in elongation when deformation level increased.

3.4 Fracture morphology

The fracture morphology of the Ni−W−Co−Ta MHA in Fig. 8(a) showed a typical ductile fracture which contained many dimples. After cryogenic rolling to 30% thickness reduction, the number of large tough dimples decreased and a small number of cleavage planes appeared (Fig. 8(b)). Plenty of tiny holes could be seen, and elongation rapidly decreased to 17.9% after rolling to 50% reduction. The number of cleavage planes continued to increase, and larger holes were formed as the degree of deformation increased (Figs. 8(c, d)). As a result, elongation of this MHA was only 9.6%. When the thickness reduction reached 90% (Fig. 8(e)), the area occupied by the cleavage planes further increased. Herein, fracture mode changed to quasi-cleavage and ductile mixed mode. Some small holes, that were elongated and linearly arranged along RD, appeared. By comparing Figs. 4 and 8, it can be seen that the micropores on the fractures were almost identical to those of insoluble W particles, which suggested that these micropores were caused by the peeling off of insoluble W particles.

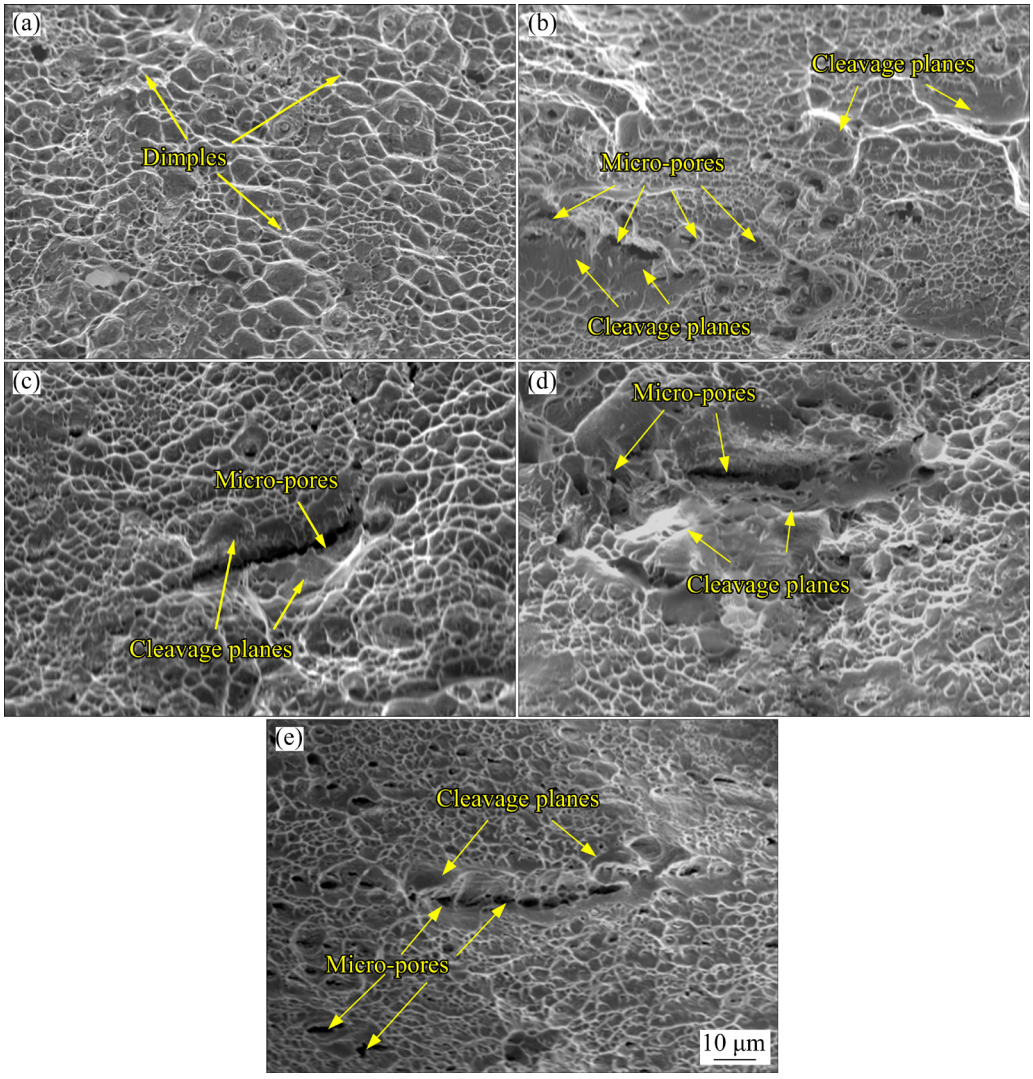

Fig. 8 Fracture morphologies of Ni−W−Co−Ta MHAs: (a) Before cryogenic rolling; (b) Rolling reduction of 30%; (c) Rolling reduction of 50%; (d) Rolling reduction of 70%; (e) Rolling reduction of 90%

4 Discussion

The microstructural evolution of Ni−W−Co−Ta MHA in Fig. 6 reveals that the deformed microstructure was mainly composed of high-density dislocations and some deformation twins at a lower degree of deformation (30%). Dislocation slips [34] and deformation twinning [35,36] are two well-known mechanisms to accommodate strain induced by plastic deformation in metallic materials. SARMA et al [37] demonstrated high-stacking fault energy (SFE) metals (e.g. Al, AA6061) coordinate deformation through dislocation slips, while low-SFE metals (e.g. Cu−Al alloys) by deformation twinning during cryogenic rolling. Both dislocation slipping and twinning mechanisms can be activated simultaneously in medium SFE (e.g. Fe−36Ni) metals [38], when the difference between the critical resolved shear stress of twinning and slip is insignificant at lower deformation levels. Hence, the appearance of deformation twins can be attributed to the following two factors in this MHA. First, Shockley partial dislocations (b=1/6{112}) swept across the continuous slip plane ({111} type) during plastic deformation of FCC metals. Layer dislocations on the crystalline surface changed the original stacking order, leading to the appearance of deformation twins [39]. Second, there are soft and hard orientation grains of Ni−W−Co−Ta MHA during plastic deformation. Individually, the soft-orientation grains are highly susceptible to slip bands, whereas the hard ones have difficulties in activating slip during plastic deformation [40]. In order to accommodate the local strain, hard-oriented grains usually have to develop deformation twinning. As a result, some of these originally unfavorable slip systems are converted to positions that are favorable for the occurrence of slipping, further stimulating slipping and crystal deformation [41].

As the level of deformation increased, the critical resolved shear stress for twinning increases much more than that for dislocation slips. The formation of twins is suppressed, and dislocation slip becomes predominant. Interaction among high-density dislocations was intensified to form dislocation walls and dislocation cells. Continuous increase in the cumulative strain further drove the formation of subgrains. Moreover, the amount of deformation twins gradually increased with increasing deformation (Fig. 6). This also indicates that deformation twins probably promote dislocation slips, suggesting that deformation of Ni−W−Co−Ta MHA is dominated by dislocation slips, whereas deformation twins play a coordinating role during rolling. A similar mechanism was found in rolled Cu−Ag alloys [42]. According to these observations, the grain refinement mechanism of Ni−W−Co−Ta MHA is mainly attributed to the proliferation and interaction of dislocations, by which the grains are gradually refined to nanocrystals (Fig. 6(f)). These nano-crystals are relatively randomly oriented. This may also be associated with grain boundary sliding that is more effective for nano-scale compared with coarse grains [43]. Meanwhile, grain rotation is another alternative way to accommodate the plastic deformation for nanocrystals, which can significantly increase misorientation and turn nanocrystals into random orientations [44].

The increase in dislocation density and grain refinement have much effect on the mechanical properties of Ni−W−Co−Ta MHA. It has been shown that solid-solution strengthening (σ_{SS}), dislocation strengthening (σ_D), grain boundary strengthening (σ_{GB}), and secondary phase strengthening (σ_{SP}) are the main mechanisms to increase the yield strength (σ) of metallic materials [45]. Usually, they satisfy the following equation:

$$\sigma=\sigma_{SS}+\sigma_D+\sigma_{GB}+\sigma_{SP} \quad (2)$$

For the Ni−W−Co−Ta MHA used in this study, significant strain hardening was observed after cryogenic rolling, which was attributed to the presence of high density of dislocations. Theoretically, the dislocation strengthening effect can be assessed according to the Taylor hardening equation [46]:

$$\sigma_D=MaGb\sqrt{\rho} \quad (3)$$

where M, a, ρ, and G denote the Taylor factor taken as 3.06, the empirical strength factor of 0.24, the dislocation density, and the shear modulus of 80.4 GPa for this Ni−W−Co−Ta MHA, respectively [24,47]. Calculated by Eq. (3), the dislocation strengthening contribution was 691 MPa at 90% thickness reduction.

Grain boundary strengthening is also crucial to

improving the strength of materials. Usually, the grain boundary strengthening is mainly related to (1) twin density and twin thickness, and (2) grain and subgrain size [42]. According to TEM analysis (Fig. 6), the density of deformation twins was low after rolling, which would be less useful for impeding dislocation movement. Therefore, the grain boundary strengthening induced by cryogenic rolling is mainly attributed to grain refinement [48]. Theoretically, it can be assessed by the Hall−Petch equation [49]:

$$\sigma_{GB}=\sigma_0+k_y d^{-1/2} \quad (4)$$

where σ_0, k_y, and d denote the intrinsic strength, the material constant, and the grain size, respectively. Similarly, σ_0 and k_y denote as 22 MPa and 0.16 MPa·m$^{-1/2}$ [50], respectively. The grain boundary strengthening contribution was about 1261 MPa at 90% thickness reduction. In summary, the theoretical yield strength of Ni−W−Co−Ta MHA after cryogenic rolling to 90% thickness reduction was 1952 MPa, which is 93 MPa different from the present experimental value. The discrepancy is likely due to the fact that the calculation adopted material characteristics of Ni instead of actual Ni−W−Co−Ta MHA in this work that was scarcely reported. Relatively smaller values of G, σ_0, and k_y would lead to this underestimation of yield strength.

5 Conclusions

(1) Cryogenic rolling significantly refined the grains to 16.1 nm after 90% thickness reduction and introduced a lot of dislocation in the investigated Ni−W−Co−Ta MHA. Some undissolved W after cryogenic rolling showed a similar morphology, i.e. elongated W, broken W, and W in a spindle shape.

(2) The plastic deformation mechanism of the Ni−W−Co−Ta MHA was determined to be dominated by dislocation slip, while co-existing deformation twins played a role in coordinating the plastic deformation.

(3) The mechanical properties were significantly improved by the deformed micro-structures induced by cryogenic rolling. The hardness, yield strength and tensile strength of Ni−W−Co−Ta MHA after cryogenic rolling to 90% thickness reduction increased to HV 590, 2107 MPa, and 2045 MPa, respectively.

(4) The fracture morphology gradually changed from typical ductile mode for the undeformed sample to quasi-cleavage and ductile mixed mode after cryogenic rolling.

CRediT authorship contribution statement

Kang-hao SHU: Conceptualization, Software, Methodology, Writing − Original draft, Formal analysis, Resources, Visualization; **Yi XIONG:** Conceptualization, Validation, Writing − Review & editing, Investigation, Funding acquisition; **Yong LI:** Conceptualization, Methodology, Validation, Resources; **Yun YUE:** Methodology, Validation, Formal analysis, Resources; **Zheng-ge CHEN:** Validation, Formal analysis, Resources; **Xiao-qin ZHA:** Formal analysis, Investigation, Data curation; **Shun HAN:** Resources, Writing − Review & editing, Visualization; **Chun-xu WANG:** Investigation, Data curation.

Declaration of competing interest

The authors declare that they have no known competing financial interests or personal relationships that could have appeared to influence the work reported in this paper.

Data availability statements

The datasets generated during and/or analyzed during the current study are available from the corresponding author on reasonable request.

Acknowledgments

This work was supported by the National Natural Science Foundation of China (Nos. U1804146, 51905153, 52111530068), the Science and Technology Innovation Team of Henan University of Science and Technology, China (No. 2015XTD006), and Major Science and Technology Project of Henan Province, China (No. 221100230200).

References

[1] PAWEL Z, RADOSLAW W, MACIEJ M, MARCIN N, ZYGMUNT P. Experimental and numerical study on the PG-7VM warhead performance against high-hardness armor steel [J]. Materials, 2021, 14(11): 3020.

[2] YUAN Shu-qiang, ZHANG Bao-yu, CHEN Zi-ming, SHANG Fu-jun. Current situation and development of tungsten alloy materials for warhead [J]. China Tungsten Industry, 2015, 30(2): 49−52. (in Chinese)

[3] TDEMIR T, UBEYLI M, YILDIRIM R O. Effect of hardness on the ballistic impact behavior of high-strength steels against 7.62 mm armor piercing projectiles [J]. Journal of Materials Engineering and Performance, 2009, 18(2): 145−153.

[4] ZHANG Jing-yu, TANG Yao, ZHOU Hui-min, CHEN Qing, ZHOU Jie, MENG Yi. Investigation on thermal rheological behavior and processing map of 30CrMnSiNi2A ultra-strength steel [J]. International Journal of Material Forming, 2020, 14(4): 507−521.

[5] ODESHI A G, BASSIM M N, AL-AMEERI S. Effect of heat treatment on adiabatic shear bands in a high-strength low alloy steel [J]. Materials Science and Engineering A, 2005, 419: 69−75.

[6] ZHANG Ji. Study on dynamic mechanical properties of shell material of high speed penetration warhead [J]. Journal of Sichuan Ordnance Engineering, 2014, 35(8): 11−14. (in Chinese)

[7] SHARMA V, NAMBURU S A S, LALWANI P, SAGAR C K. Constitutive modelling and processing map analysis of tungsten heavy alloy (92.5W−5.25Ni−2.25Fe) at elevated temperatures [J]. International Journal of Refractory Metals & Hard Materials, 2018, 76: 168−179.

[8] CHUVILDEEVA V N, NOKHRINA A V, BOLDINA M S, SAKHAROVA N V, BARANOVB G V. Influence of high-energy ball milling on the solid-phase sintering kinetics of ultrafine-grained heavy tungsten alloy [J]. Doklady Physics, 2017, 62(9): 420−424.

[9] KIRAN U R, KUMAR J, KUMAR V, SANKARANARAYANA M, RAO G V S N, NANDY T K. Effect of cyclic heat treatment and swaging on mechanical properties of the tungsten heavy alloys [J]. Materials Science and Engineering A, 2016, 656: 256−265.

[10] CHEN X, XIE Z M, XIE X F, ZENG L F, LIU R, YANG J F, WU X B, WANG X P, LIU C S, FANG Q F. Achieving a remarkable low-temperature tensile ductility in a high-strength tungsten alloy [J]. Tungsten, 2024, 6(1): 150−161.

[11] KIRAN U R, VENKAT S, RISHIKESH B, IYER V K, SANKARANARAYANA M, NANDY T K. Effect of tungsten content on microstructure and mechanical properties of swaged tungsten heavy alloys [J]. Materials Science and Engineering A, 2013, 528: 389−396.

[12] PRABHU G, KUMAR N A, SANKARANARAYANA M, NANDY T K. Tensile and impact properties of microwave sintered tungsten heavy alloys [J]. Materials Science and Engineering A, 2014, 607: 63−70.

[13] SENTHILNATHAN N, ANNAMALAI A R, VENKATACHLAM G. Microstructure and mechanical properties of spark plasma sintered tungsten heavy alloys [J]. Materials Science and Engineering A, 2018, 710: 66−73.

[14] ZUO Geng, CUI Nan-nan, LI Xiao-jie, WEN Shao-bo, ZHENG Hong-jun. Analysis and guarantee suggestion of advantage metal mineral industry in our country-take tungsten, antimony and rare earth as examples [J]. Natural Resource Economics of China, 2022, 35(10): 11−17, 38. (in Chinese)

[15] YE Lei, HAN Yong, FAN Jing-lian, DU Zhi-yuan. Fabrication of ultrafine-grain and great performance W−Ni−Fe alloy with medium W content [J]. Journal of Alloys and Compounds, 2020, 846: 156237.

[16] NIE H, ZHANG T. Development of manufacturing technology on WC−Co hardmetals [J]. Tungsten, 2019, 1(3): 198−212.

[17] LI Y, LIU G Q, HU X B, Wu L H, TAN C W, DRAVID V P, LIU S Z. A novel medium heavy alloy with superior quasi-static and dynamic properties [J]. Scripta Materialia, 2019, 162: 311−315.

[18] MENG Y, REN Q, JUN X H. Dislocation density in deformed metals is measured by local disorientation [J]. Transactions of Metal Heat Treatment, 2016, 35(11): 122−128. (in Chinese)

[19] KONKOVA T, MIRONOV S, KORZNIKOV A, SEMIATIN S L. microstructural response of pure copper to cryogenic rolling [J]. Acta Materialia, 2010, 58: 5262−5273.

[20] XIONG Y, HE Tian-tian, WANG Jun-bei, LU Yan, CHEN Lu-fei, REN Feng-zhang, LIU Yu-liang, VOLINSKY A A. Cryorolling effect on microstructure and mechanical properties of Fe−25Cr−20Ni austenitic stainless steel [J]. Materials & Design, 2015, 88: 398−405.

[21] SELVAN C C, NARAYANAN C S, VIGNESHWARAN S, NARAYANASAMY R. The microstructure transformations and deformation behavior of Al−4Mg−0.2Zr alloy rolled at ambient and cryogenic temperatures [J]. Materials Research Express, 2019, 6(10): 1065a5.

[22] ABBASI-BAHARANCHI M, KARIMZADEH F, ENAYATI M H. Thermal stability evaluation of nanostructured Al6061 alloy produced by cryorolling [J]. Transactions of Nonferrous Metals Society of China, 2017, 27(4): 754−762.

[23] MA Yun-fei, XIONG Yi, CHEN Zheng-ge, ZHA Xiao-qin, HE Tian-tian, LI Yong, SINGH H, KOMI K, HUTTULA M, CAO Wei. Microstructure evolution and properties of gradient nanostructures subjected to laser shock processing in 300M ultrahigh-strength steel [J]. Steel Research International, 2021, 93(2): 2100434.

[24] CHENG H, WANG H Y, XIE Y C, TANG Q H, DAI P Q. Controllable fabrication of a carbide-containing FeCoCrNiMn high-entropy alloy: Microstructure and mechanical properties [J]. Materials Science and Technology, 2017, 33(17): 2032−2039.

[25] ZHOU Tian, XIONG Yi, YUE Yun, LU Yan, CHEN Yan-na, HE Tian-tian, REN Feng-zhang, SINGH H, KOMIB J, HUTTULA M, CAO Wei. Controlled cold rolling effect on microstructure and mechanical properties of Ce-modified SAF 2507 super duplex stainless steel [J]. Materials Science and Engineering A, 2019, 766: 138352.

[26] ZHENG Han, FU Li-ming, JI Xin-bo, DING Yi, WANG Wei, MAO Wen, SHAN Ai-dang. Microstructural evolution and mechanical property of ultrafine-grained pearlitic steel by cold rolling: The influence of cementite morphology [J]. Materials Science and Engineering A, 2021, 824: 141860.

[27] TORIBIO J, OVEJERO E. Effect of cumulative cold drawing on the pearlite interlamellar spacing in eutectoid steel [J]. Scripta Materialia, 1998, 39(3): 323−328.

[28] UEJIA R, TSUJI N, MINAMINO Y, KOIZUMI Y. Ultragrain refinement of plain low carbon steel by cold-rolling and annealing of martensite [J]. Acta Materialia, 2002, 50: 4177−4189.

[29] PANIGRAHI S K, JAYAGANTHAN R. Development of ultrafine grained high strength age hardenable Al 7075 alloy by cryorolling [J]. Materials & Design, 2011, 32: 3150−3160.

[30] LI Jun-chen, LUO Xiao-xia, MA Guo-cai, WANG Jun-wei. The effect of cold rolled reduction ratios on grain boundary character and mechanical properties of the SUS301L austenitic stainless steel [J]. Materials Research Express, 2019, 6(12): 126587.

[31] ZHANG Jia-long, LU Li-wei1, CHE Bo, LI Min-ha, MA Min, YANG Yan. Effects of cryogenic treatment on microstructure and mechanical properties of Mg alloy under variable paths rolling [J]. The Chinese Journal of Nonferrous Metals, 2022, 32(11): 3280−3293. (in Chinese)

[32] MEYERS M A, VOHRINGER O, LUBARDA V A. The onset of twinning in metals: A constitutive description [J].

Acta Materialia, 2001, 49: 4025−4039.
[33] CHEN Ming-wei, MA En, HEMKER K J, SHENG Hong-wei, WANG Yin-min, CHENG Xue-mei. Deformation twinning in nanocrystalline aluminum [J]. Science, 2003, 300(5623): 1275− 1277.
[34] WELSCH E, PONGE D, HAGHIGHAT S M H, SANDLOBES S, CHOI P, HERBIG M, ZAEFFERER S, RAABE D. Strain hardening by dynamic slip band refinement in a high-Mn lightweight steel [J]. Acta Materialia, 2016, 116: 188−199.
[35] HENDRAWAN C N, SETYANI A, PERTIWI D R K, SOFYAN B T. Effect of 9 wt.% Mn addition on cold rolling and annealing behaviour of Cu−31Zn alloy [J]. Material Today: Proceedings, 2021, 46(9): 3346−3351.
[36] HWANG J K. Effects of caliber rolling on microstructure and mechanical properties in twinning-induced plasticity (TWIP) steel [J]. Materials Science and Engineering A, 2018, 711: 156−164.
[37] SARMA V S, WANG J, JIAN W W, KAUFFMANN A, CONRAD H. Role of stacking fault energy in strengthening due to cryo-deformation of FCC metals [J]. Materials Science and Engineering A, 2010, 527: 7624−7630.
[38] ZHENG Jian-jun, LI Chang-sheng, HE Shuai, CAI Ban. Deformation behavior of Fe−36Ni steel during cryogenic (123−173 K) rolling [J]. Journal of Iron and Steel Research International, 2016, 23(5): 447−452
[39] ZHU Y T, WU X L, LIAO X Z, NARAYAN J, KECSKÉS L J, MATHAUDHU S N. Dislocation-twin interactions in nanocrystalline FCC metals [J]. Acta Materialia, 2011, 59: 812−821.
[40] WANG L, YANG Y, EISENLOHR P, BIELER T R, CRIMP M A, MASON D E. Twin nucleation by slip transfer across grain boundaries in commercial purity titanium [J]. Acta Materialia, 2011, 59: 812−821.
[41] YOO M H, MORRIS J R, HO K M, AGNEW S. R. Nonbasal deformation modes of HCP metals and alloys: Role of dislocation source and mobility [J]. Metallurgical and Materials Transactions A, 2002, 33(3): 813−822.
[42] XIE Ming-wang, HUANG Wei, CHEN Hui-ming, GONG Liu-kui. Microstructural evolution and strengthening mechanisms in cold-rolled Cu−Ag alloys [J]. Journal of Alloys and Compounds, 2020, 851: 156893.
[43] SWYGENHOVEN H V, FARKAS D, CARO A. Grain-boundary structures in polycrystalline metals at the nanoscale [J]. Physical Review B, 2000, 62: 831−838.
[44] HELLSTERN E, FECHT H J, FU Z, JOHNSON W L. Structural and thermodynamic properties of heavily mechanically deformed Ru and AlRu [J]. Journal of Applied Physics, 1989, 65: 305−310.
[45] TONG Yun-xiang, LI Si-yuan, ZHANG Dian-tao, LI Li, ZHENG Yu-feng. High strength and high electrical conductivity CuMg alloy prepared by cryorolling [J]. Transactions of Nonferrous Metals Society of China, 2019, 29(3): 595−600.
[46] HE B, HU B, YEN H, CHENG G, WANG Z. High dislocation density-induced large ductility in deformed and partitioned steels [J]. Science, 2017, 357(6355): 1029−1032.
[47] LI Li-li, HAN Ming. Shear behaviors of single crystal nickel at different temperatures: Molecular dynamics simulations [J]. Applied Physics A: Materials Science and Processing, 2015, 119(3): 1101−1107.
[48] WU X X, SAN X Y, LIANG X G, GONG Y L. Effect of stacking fault energy on mechanical behavior of cold-forging Cu and Cu alloys [J]. Material & Design, 2013, 47: 372−376.
[49] LIU Shuo, ZHANG Fu-cheng, YANG Zhi-nan, WANG Ming-ming, ZHENG Chun-lei. Effects of Al and Mn on the formation and properties of nanostructured pearlite in high-carbon steels [J]. Material & Design, 2016, 93: 73−80.
[50] SRIHARITHA R, MURTY B S, KOTTADA R S. Alloying, thermal stability and strengthening in spark plasma sintered AlxCoCrCuFeNi high entropy alloys [J]. Journal of Alloys and Compounds, 2014, 583: 419−426.

深冷轧制变形对新型 Ni−W−Co−Ta 高密度合金显微组织与性能的影响

舒康豪[1]，熊 毅[1,2]，厉 勇[3]，岳 赟[1]，陈正阁[4]，查小琴[5]，韩 顺[3]，王春旭[3]

1. 河南科技大学 材料科学与工程学院，洛阳 471023；
2. 有色金属新材料与先进加工技术省部共建协同创新中心，洛阳 471023；
3. 钢铁研究总院 特殊钢研究所，北京 100081；
4. 西北核技术研究所 激光与物质相互作用国家重点实验室，西安 710024；
5. 中国船舶重工集团第 725 研究所，洛阳 471000

摘 要：采用熔炼−浇铸−锻造流程制备新型 Ni−W−Co−Ta 高强度合金，并对 Ni−W−Co−Ta 合金经深冷轧制变形后的显微组织及力学性能演变规律进行表征。结果表明：随着变形量的增加，新型 Ni−W−Co−Ta 高密度合金中等轴晶粒沿轧制方向不断被拉长，同时产生大量的滑移带以协调剧烈的塑性变形，并最终形成纤维组织。变形量的增大导致位错密度急剧增大，位错交互作用显著加强，进而使晶粒尺寸细化至纳米量级；合金强度、硬度随着变形量的增加而显著提高，伸长率则急剧下降。断口形貌则由韧性断裂(未变形)向准解理−韧性混合型断裂转变(90%变形量)。

关键词：Ni−W−Co−Ta 高密度合金；深冷轧制；纤维组织；力学性能；准解理−韧性混合型断裂

(Edited by Bing YANG)